

DOI: <https://doi.org/10.15407/rpra30.04.217>
UDC 52.77+523.3-1/-8

A.L. Sukharev, M.I. Ryabov, V.V. Galanin, D.A. Zabora
Observatory "URAN-4", Institute of Radio Astronomy NAS of Ukraine
1v, Marazliivska St., Odesa, 65014, Ukraine
E-mail: uran4@te.net.ua

IMPACT OF THE NOVEMBER 3, 2013 SOLAR ECLIPSE ON THE STATE OF THE IONOSPHERE AS INVESTIGATED IN A RADIO ASTRONOMICAL TECHNIQUE

Subject and Purpose. This work examines effects of the November 3, 2013 solar eclipse, in particular the atypical increases in the level of radio interference and scintillations of the radio sources 3C 123 and Cas-A that were observed at 25 MHz. These phenomena might owe to the enhanced wave activity in the ionosphere during the eclipse and a reduced radio wave absorption.

Methods and Methodology. The observations were conducted with the use of the low-frequency radio telescope URAN-4 (operative range 10–30 MHz). The observational data concerning radiation from cosmic radio sources and the accompanying interference are presented, for further analysis, in the form of time series. Wavelet analysis has been applied to the data arrays to identify the dominant periods of radio source scintillation.

Results. A significant increase in interference intensity was observed on the day of the eclipse climax, as well as the next day. The radio source Cas-A exhibited quasi-periodic variations of intensity on a timescale of 3 to 7 minutes. The scintillation analysis performed for the source 3C 123 before and after the eclipse failed to provide conclusive evidence of eclipse-related effects.

Conclusions. Despite the fact that the solar eclipse of November 3, 2013, was not optically visible in Ukraine (because the nearest visibility zone for the partial eclipse lay farther toward the South of the Crimea and further on toward Turkey), an anomalous rise in the level of interference was still recorded over the time window of observations from October 31 to November 7, 2013. No similar enhancements were observed either before or after the eclipse. This is likely the result of a combined effect involving reduced absorption in the ionospheric D-layer, the noticeable shift in the F-layer's location (which leads to appearance of distant reflections), and appearance of active agents like TIDs. All of these together brought forth a sharp increase in interference levels at 25 MHz. Despite the fact that the eclipse stayed optically invisible, its generated ionospheric disturbances proved capable of reaching the URAN-4 facility, manifesting themselves through a strong burst of interference during zenith-oriented reception.

Keywords: radio scintillations, ionosphere, ionospheric storm, geomagnetic storm, solar eclipse manifestations in the ionosphere, decameter-wavelength radio astronomy.


Introduction

The analysis of archival data on flux variations of cosmic sources during solar eclipses, accumulated over the operational period of the URAN-4 radio telescope [1], presents considerable scientific interest.

This study of the solar eclipse that occurred on November 3, 2013 initiates a broader research program focused on ionospheric effects of solar eclipses in the decameter wavelength range, which makes use of both archival and contemporary data obtained with the URAN-4.

Citation: Sukharev, A.L., Ryabov, M.I., Galanin, V.V., Zabora, D.A., 2025. Impact of the November 3, 2013 solar eclipse on the state of the ionosphere as investigated in a radio astronomical technique. *Radio Phys. Radio Astron.*, 30(4), pp. 217–231. <https://doi.org/10.15407/rpra30.04.217>

© Publisher PH "Akademiya" of the NAS of Ukraine, 2025

 This is an Open Access article under the CC BY-NC-ND 4.0 license (<https://creativecommons.org/licenses/by-nc-nd/4.0/legalcode.en>)

Particular emphasis is placed on the investigation of scintillations of cosmic radio sources and variations in the intensity of external radio-frequency interference during periods of solar eclipse-induced ionospheric disturbances. During an eclipse, the flow of ionizing radiation from the Sun toward the Earth is temporarily blocked, which results in abrupt changes in temperature, pressure, an electron density in the upper atmosphere. These changes generate wave-like disturbances that may resemble ionospheric storms, with some of their similar effects. However, normally they demonstrate lower intensity and are shorter in duration than those caused by solar activity. A detailed review of such phenomena is provided in the paper by L.F. Chernogor [2]. Another potentially significant effect associated with solar eclipses concerns the solar wind – lunar environment interaction. An effect of importance may be formation of the so called "solar wind shadow" which is oriented toward the Earth during the eclipse. This interaction may serve as an additional source of disturbances, both in the magnetosphere and ionosphere.

Studies of solar eclipse-induced effects in the ionosphere have been conducted for many years, primarily with the use of ionosondes or else, through measurements of scintillating GPS signals with satellite-based receivers. Meanwhile, some noticeable advantages may be obtainable by appealing to radio astronomical methods. Specifically, the detection of ionospheric scintillations of cosmic radio sources (and of the accompanying interference) with the use of phased antenna arrays operating in the decimeter range (10–30 MHz) offers distinct advantages. This approach enables continuous, long-duration observations without the need for active probing, by means of tracking ionospheric changes over extended time scales. The large aperture and high sensitivity of the phased array facilitate detection of fine-scale turbulent and wave structures in the ionosphere that might have remained undetectable for ionosondes. The high level of time resolution of the output data (specifically, 1 sample per second provided by the URAN-4) allows for constructing detailed time-frequency spectra, thus clearly revealing the fine structure of the received signals.

The objective of this study has been to investigate the effects of the solar eclipse on the propagation of decimeter wavelength radio emissions through the ionosphere and the associated changes in the inter-

ference environment. The methodology is based on passive probing of the ionosphere by powerful cosmic radio sources. The effects under observation reveal differences in interference intensity before and during the eclipse, as well as changes in the shape and structure of the wavelet spectra of the ionospheric scintillations. During a solar eclipse, the appearance of global disturbances in the ionosphere is driven by the solar ultraviolet and X-ray radiation whose intensity is modulated by the Moon. Additionally, the Moon alters the dynamics of solar wind interaction with the terrestrial magnetosphere, which may also lead to emergence of wave-like disturbances in the ionosphere.

According to the data from the Explorer-35 and Explorer-33 spacecraft [3], a hollow region was detected in the lunar orbit, which followed the Moon itself and where particle density was tens of times lower than in the surrounding solar wind. This cavity takes the form of a cone, with its opening angle determined by the Mach angle. The resulting magnetic field geometry in the solar wind's portion flowing around the Moon is rather complex and highly sensitive to solar wind parameters and the interplanetary magnetic field's configuration. Studies by Ness [4] on solar wind – Moon interactions have revealed a shadow region which is formed behind the Moon in the solar wind and consists of a plasma cavity and a penumbral zone. This interaction brings forth intense magnetic fluctuations in the solar wind (within the near-Earth space). An interruption, during a solar eclipse, of the solar wind flow into the sector behind the Moon may affect the solar wind – magnetosphere coupling and electrodynamic processes in the ionosphere [5].

This study examines the effects of the total solar eclipse of November 3, 2013, making use of the results of observations of scintillations from strong cosmic radio sources and variations in interference intensity of the decimeter-wavelength radiation recorded with the URAN-4 radio telescope of the Institute of Radio Astronomy, NASU. Solar eclipses induce substantial restructuring of the ionosphere. For instance, the solar eclipse of January 4, 2011 led, as demonstrated in paper [6], to a significant reduction in electron concentration within the middle ionosphere. At the peak of layer F2, the relative decrease in electron density reached approximately 52%. During the eclipse, ionograms appeared blurred, in-

dicating a pronounced ionospheric turbulence. The eclipse was also accompanied by an increase in the relative amplitude of quasi-periodic variations in electron concentration—approximately twice the magnitude typical of an ordinary day, in other words 8 and 16%, respectively, for the oscillation periods of 30 and 60 minutes. The oscillation periods varied, and the parameters of the quasi-periodic disturbances were consistent with those of internal gravity waves.

This work has been aimed at identifying the ionospheric effects that occur at considerable distances from the area of total eclipse, specifically at the farthest locations of the URAN-4 radio telescope.

The observational targets in this study include the interference superimposed on the galactic radio background [7, 8] and the radiation from cosmic radio sources 3C 123 and Cas-A. The 3C 123 (a radio galaxy) and Cas-A (a supernova remnant) used to be routinely monitored by the URAN-4 radio telescope, typically on a daily basis. These two sources have been widely used for studying ionospheric scintillations across all Ukrainian antennas of the URAN system, as well as with international phased arrays, such as LOFAR.

A notable example is the investigation conducted in Ahmedabad, India during the solar eclipse of August 11, 1999 [9], which documented an increased intensity of radio interference and enhanced level of scintillation of cosmic sources. The effects have been attributed to reduced ionospheric absorption and extended propagation paths for the signals from distant radios. In contrast, the fact that the solar eclipse of November 3, 2013 was not optically visible from the Ukrainian territory presents a compelling scientific opportunity to explore remote manifestations of eclipse-induced effects in the Earth's ionosphere.

1. Observational methods and data processing techniques

The low-frequency radio telescope URAN-4 (operational since 1987) is a phased antenna array with electronic beam steering. The antenna consists of 128 pairs of dipoles arranged on a site measuring 232.5×22.5 meters and oriented along the East—West direction. This configuration enables reception in two linear polarizations, designated like A and B. At a frequency of 25 MHz, the antenna pattern mea-

sures as $2.7^\circ \times 22^\circ$. The URAN-4 is one of the constituent elements of the national low-frequency radio interferometry system designated as URAN, Ukraine. The observational data were obtained using a hardware complex that includes a modernized antenna control unit and a radiometer for registering the radio emissions of interest (the radiometer was designed and constructed by V.V. Galanin of the Institute of Radio Astronomy, NASU). Our observations were carried out at the frequencies of 20 and 25 MHz.

During the experiment, the radiometer was operated in both the total power and modulation modes. The antenna array's configuration specific for our experiments was implemented as two halves of the URAN-4.

The resulting observation files contain time data (Julian calendar dates), total power at each of the two observable frequencies (namely, 20 and 25 MHz), for two linear polarizations (P), as well as signals at difference frequencies from the two antenna halves. The primary operating mode was the modulation mode (P_M).

The monitoring program of spectral flux densities of strong radio sources was initiated by two of the present authors (M.I. Ryabov and V.V. Galanin [10]) at the time of URAN-4 commissioning and has been ongoing till the present day.

Spectral flux densities of the radio sources and their scintillations were monitored in the mode of multiple transits of the sources across the antenna pattern [11]. The intensities of the input signals were recorded in an output file, in terms of relative magnitudes (decibels, dB), with reference to a highly stable noise generator calibrated in antenna temperatures (Kelvin, K). The signal amplitudes at each of the calibration procedure steps were determined experimentally from test observations for each radio source belonging to the sample that is measured.

The sampling rate established for the output data file (which contained sums and differences of the signals at 20 and 25 MHz coming from the two antenna halves) equaled 1 Hz. To reveal the ionospheric scintillations, a semi-automatic pre-processing procedure was developed and implemented, followed by construction of digital time-frequency spectra through application of the fast continuous wavelet transform (CWT) [12].

The processing of observational data included stages as follows:

1) Removal of strong radio interference records and random outliers. These often appeared as "clouds" of points above and below the radio signal record. In the case of galactic background measurements, which in the decameter range are typically contaminated by numerous high-amplitude random interferences, a simple outlier removal method was applied using the Chi^2 distribution. For each data point, the deviation between the observed and expected value (median or moving average) was calculated and normalized by the expected value. If the Chi^2 statistic exceeded a critical threshold (taken from a Chi^2 distribution table), the point was classified as an outlier. The threshold depended on the chosen level of significance (typically 95 or 99%). Outliers could be excluded — either replaced by interpolated values, or smoothed out; in the present case, they were removed and the data were subsequently smoothed and interpolated with the use of a cubic spline. As a result, the main noise component in the form of a "cloud" of points was eliminated.

2) Smoothing of radio source scans. Depending on the noise level, three approaches were employed:

- In the case of a fairly low noise level the Savitzky–Golay filter [13] was used.

- If the noise level was rather high, plus the signal contained a weak pulsed interference component, the data were smoothed via application of a cubic spline, with the smoothing level determined automatically within a cross-validation procedure [14]. This method allowed reliable extraction of radio source scans and flux density variations, even in the presence of noise bursts lasting for tens of minutes.

- For strongly contaminated data with long-duration interference, the LOESS method (Locally Estimated Scatterplot Smoothing), implemented as a locally weighted least-squares procedure with a Gaussian weighting function [15], was used. This approach enabled detection of scintillations even under conditions of prolonged interference, which is not uncommon at the URAN-4 site.

3) Trend removal. To more effectively study ionospheric scintillations, the trend in the records caused by the antenna beam pattern was removed. This was complicated by the fact that the observed scans of radio sources often deviated from the form predicted theoretically, due to interference. In this work, the primary method for isolating scintillations was FFT filtering with a Hamming spectral window [16, 17].

The spectral window was applied to reduce spectral leakage, thereby enabling extraction and reconstruction of the components of low spectral power. This allowed even weaker scintillations to be clearly distinguishable against the noise background. The Hamming window does not fully decay to zero at its edges, and typically the filter can restore the full data range, with edge effects limited to about 1% at the beginning and end of the time series.

4) Estimating scintillation periods. Upon completing the above described pre-processing and normalization procedures, the principal periods of radio source scintillations were determined. In low-frequency radio astronomy, the standard practice is to use the Short-Time Fourier Transform (STFT) method (see, e.g., [18]). Meanwhile, it is subject to several limitations, such as dependence of the spectrogram appearance on the window width and overlapping. Therefore, the CWT was additionally employed, computed via FFT for analytically defined wavelets (e.g., Morlet and Gauss–Derivative) (cf. a comparative review in [19]). The visualization relied on a variety of magnitude representations, specifically $\sqrt{R^2 + I^2}$; Surface Integrals Sum Squared Amplitude Power (PSD-SSA), $2(R^2 + I^2)$, and decibels (dB) defined as $10 \log_{10}(R^2 + I^2)$, where R stands for the real and I for the imaginary part of the wavelet transform.

5) To observe variations in interference intensity superimposed on the galactic background, the URAN-4 antenna beam was directed toward the zenith. An almost continuous observation session was conducted from October 31 to November 7, 2013.

Features of the CWT with Morlet and Gauss–Deriv wavelets (the Gauss–Deriv is a wavelet based on the Gaussian function's derivative) [20]:

1) The time–frequency resolution is superior compared with the STFT method. Let us examine this statement in more detail: the STFT subdivides the time–frequency plane into a set of uniform rectangular cells. In contrast, the CWT generates a grid with cells that are narrow and elongated at the lower end (low frequencies), while being wider and compressed at the upper end (higher frequencies). This structure aligns well with the nature of most real-world signals: low-frequency processes tend to be slow, while high-frequency processes are fast.

Suppose we need to construct a signal spectrum within a 10 MHz bandwidth (15–25 MHz), centered

at 20 MHz, with a sampling rate of 10 MHz. A comparison of the STFT and CWT methods is presented in Table. In this example, we have used a Morlet wavelet characterized by a quality factor of $Q = 10$. (the Q -factor is defined here as the ratio of the wavelet's central frequency to its bandwidth, $Q = f_c / \Delta f$). The magnitude of this parameter results from the amount of compromise between the frequency resolution and time resolution that can be allowed in the process of signal analysis.

As shown in Table, the STFT method, if employed with a window of 256 samples in size, provides good temporal resolution; however, its frequency resolution remains insufficient for distinguishing between two signal components if their frequency separation is less than approximately 39 kHz. With a window size of 4096 samples, events shorter than $\sim 410 \mu\text{s}$ become smeared, and the improved frequency resolution can be achieved at the expense of a significant loss in temporal resolution.

In contrast, the CWT offers a frequency-dependent resolution. For illustration, the frequencies of 500 kHz and 4.5 MHz were considered. Unlike STFT, which requires a single compromise between time and frequency resolution for the entire analysis, CWT adapts automatically: at high frequencies, it provides exceptional temporal resolution ($2.2 \mu\text{s}$), enabling the detection of very short impulses — something STFT cannot achieve when configured for high frequency resolution. As frequency decreases, CWT sacrifices temporal resolution in favor of frequency resolution, adapting to the slower dynamics of low-frequency signals.

2) The Morlet and Gauss–Deriv wavelets exhibit excellent localization properties in both time and frequency domains, unlike STFT, where resolution is fixed for a given window size.

3) The CWT enables multi-scale signal analysis, which is particularly advantageous for studying non-stationary signals with rapid variations in amplitude, frequency, and phase.

4) Unlike STFT, which uses a fixed window width, CWT can adaptively stretch the analyzing function at low frequencies and compress it at higher frequencies. This allows for clear representation of both low-frequency and fast signal variations on the time–frequency spectrum. For this reason, CWT was employed in the present study to analyze ionospheric scintillation data from cosmic radio sources.

Comparison of the frequency- and time-resolution approaches to signal analysis within a 10 MHz bandwidth (15–25 MHz) centered at 20 MHz

Method	Analyzed frequency	Time resolution (μs)	Frequency resolution (kHz)
STFT (window 256)	Any	25.6	39.1
STFT (window 4096)	Any	409.6	2.44
CWT ($Q = 10$)	Low (500 kHz)	20	50
CWT ($Q = 10$)	High (4.5 MHz)	2.2	450

5) One of the main limitations of CWT is the variability of results depending on the choice of analyzing wavelet. In this study, two wavelets were used: the Morlet wavelet — a Gaussian modulated by a sinusoid — and the Gauss–Deriv wavelet, whose smoothness and symmetry provide good noise resistance. Although its frequency resolution is slightly inferior to that of the Morlet wavelet, it offers improved detection of short-duration bursts in the data. These wavelets are widely used in digital spectral analysis of radio astronomical, geophysical, and meteorological data. Their balanced time–frequency resolution makes them well-suited for analyzing ionospheric variations in signals from cosmic sources.

The Gauss–Deriv wavelet was applied to analyze scintillations from the radio source 3C 123, while the Morlet wavelet was used to examine the variations in Cas-A, providing a clearer visualization of quasi-periodic structures in the wavelet spectrum.

2. Conditions on the day of Total Solar Eclipse (November 3, 2013)

2.1. Space weather conditions

The total solar eclipse of November 3, 2013 occurred during the peak phase of Solar Cycle 24. According to WEEKLY [21]. The days preceding the eclipse were marked by frequent and intense solar flares, predominantly of classes M and X. On the day of the eclipse, an M5.0-class flare was recorded, reaching its peak at 05:22 UTC.

Key space weather parameters on the day of the eclipse included: Wolf sunspot number: 142; Solar radio flux at 10.7 cm ($F_{10.7}$): 142 solar flux units (SFU); Solar wind speed (V): 367 km/s; Proton den-

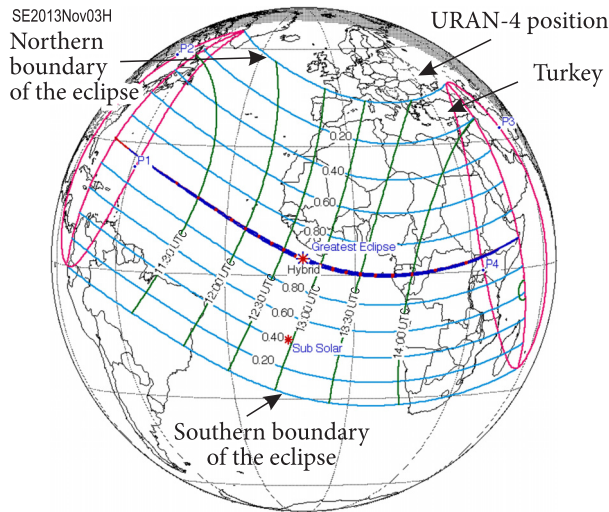


Fig. 1. Map of the path of the total solar eclipse of November 3, 2013. Credit: Eclipse Predictions by Fred Espenak, NASA's Goddard Space Flight Center (GSFC)

sity in the solar wind (P): 2.9 protons/cm³; Maximum southward component of the interplanetary magnetic field (B_z): -5 nT at 04:25 UTC. Geomagnetic field disturbances during the eclipse varied from quiet to storm-level conditions, particularly at high latitudes.

2.2. Eclipse visibility

The solar eclipse of November 3, 2013 was one of the rare hybrid eclipses, characterized by an initial annular phase which gradually transformed to totality. The eclipse was visible across the northern and central regions of the Atlantic Ocean, as well as in numerous African countries. The passage of the lunar shadow began at 10:04:34 UTC, with total phases occurring between 11:05:17 and 14:47:42 UTC. The eclipse came to an end at 15:28:21 UTC, with the maximum eclipse having occurred at 12:47:36 UTC and stayed for 1 minute and 40 seconds (<https://eclipsewise.com/solar/SEprime/2001-2100/SE-2013Nov03Hprime.html>). The zone of maximum eclipse was located outside the territory of Ukraine. At sunrise, partial phases were observable along the US East coast and in Canada, as well as on islands in the Caribbean and in the northern part of South America, including much of Brazil. By mid-day, the penumbral band extended across the entire African continent and southern Europe. In the evening hours, the partial eclipse zone passed along the Black Sea coast and through regions of Turkey and the Middle East. Thus, the "influence zone" of the

processes associated with the trace of the total phase spanned from equatorial to mid-latitude regions. A map of the total solar eclipse of November 3, 2013 is shown in Fig. 1 [22].

3. Results

3.1. Solar eclipse manifestations as revealed by interference observations at decameter radio wavelengths

Observations of radio-frequency interference superimposed on the low-frequency galactic background were conducted with the URAN-4 antenna beam directed toward zenith, which regime corresponded to the maximum effective area of the antenna. The full-power mode was employed, summing up the signals from both sub-antennas. Recording intervals were as follows: 10:46–19:00 GMT on November 2, 2013; 07:29–19:15 GMT on November 3 (date of the eclipse: total duration 11 hours 46 minutes); and 08:07–19:42 GMT on November 4, 2013. The results of interference measurements at 25 MHz (linear polarization A) are presented in Fig. 2. The figure presents smoothed recordings of the galactic radio background, with superimposed high-intensity interference at a frequency of 25 MHz (total power presented in terms of ADC counts), that were obtained on the control day prior, and after, to the solar eclipse. It is evident that, compared to the control day, the interference intensity increased significantly on the day of the eclipse and remained elevated on the day after. These data have undergone preliminary processing, including removal of a substantial array of randomly off-set points, and data smoothing with the use of the Savitzky–Golay polynomial filter and cubic spline interpolation. The processed results clearly show that interference intensity on the day of the solar eclipse was significantly higher than on the days before and after the climax.

The complete set of raw (unprocessed) data on the full-power signal (linear polarization A) at 20 MHz is shown in Fig. 3. The dataset includes contributions from the galactic background, cosmic radio sources, and high-amplitude radio-interference. It is evident that on November 3, 2013 — the day of the solar eclipse — the peak interference level was approximately 1.8 times higher (in ADC counts, corresponding to voltage: ~5 dB) than on the day following the eclipse, November 4. Overall, the interference level

on November 3 exceeded that of the other four observation days. These data fully confirm that on November 3, 2013 interference was markedly stronger than on any other day of observations, and that the interference level on November 4 remained elevated compared to November 2, 5, and 6. This suggests persistence of a residual, mildly excited ionospheric state even on the day following the eclipse.

Such effects, occurring during either a total or partial solar eclipse, and resulting from abrupt reductions in photo-ionization in the upper atmosphere lead to changes in ionospheric absorption and reflection of HF signals (3–30 MHz) – even at hundreds of kilometers away from the lunar shadow zone. Similar phenomena have previously been observed as increased interference levels and detection of weak signals from distant radios, apparently non-detectable on control days during various solar eclipses.

A distinctive feature of the November 3, 2013 eclipse observations at URAN-4 is that the edge of the lunar penumbra passed approximately 270 kilometers south of the village of Mayaky. This allows for the hypothesis that the eclipse, although not optically visible from Ukraine, generated extended ionospheric disturbances that propagated well beyond the boundary of the optical penumbra. At the point of maximum eclipse (in the Atlantic Ocean, south of Liberia), the width of the total shadow path was 58 km, while the penumbral width during peak eclipse reached approximately 6800 km, covering a substantial portion of the Atlantic Ocean, the entire African continent, southern Europe, and parts of the Middle East.

A detailed analysis of ionospheric absorption reduction during the solar eclipse of February 16, 1980 in India is presented in study [23]. Observational data from the solar eclipse of August 11, 1999 revealed that electron density in the ionosphere significantly decreased not only within the path of totality, but also within the penumbral region, where electron concentrations in both the F and E layers dropped by 20–35% [24].

Furthermore, it is now well established that solar eclipses can act as sources of acoustic-gravity waves and strong meridional atmospheric flows. Such disturbances are capable of propagating through the ionosphere over considerable distances from their origin [25, 26].

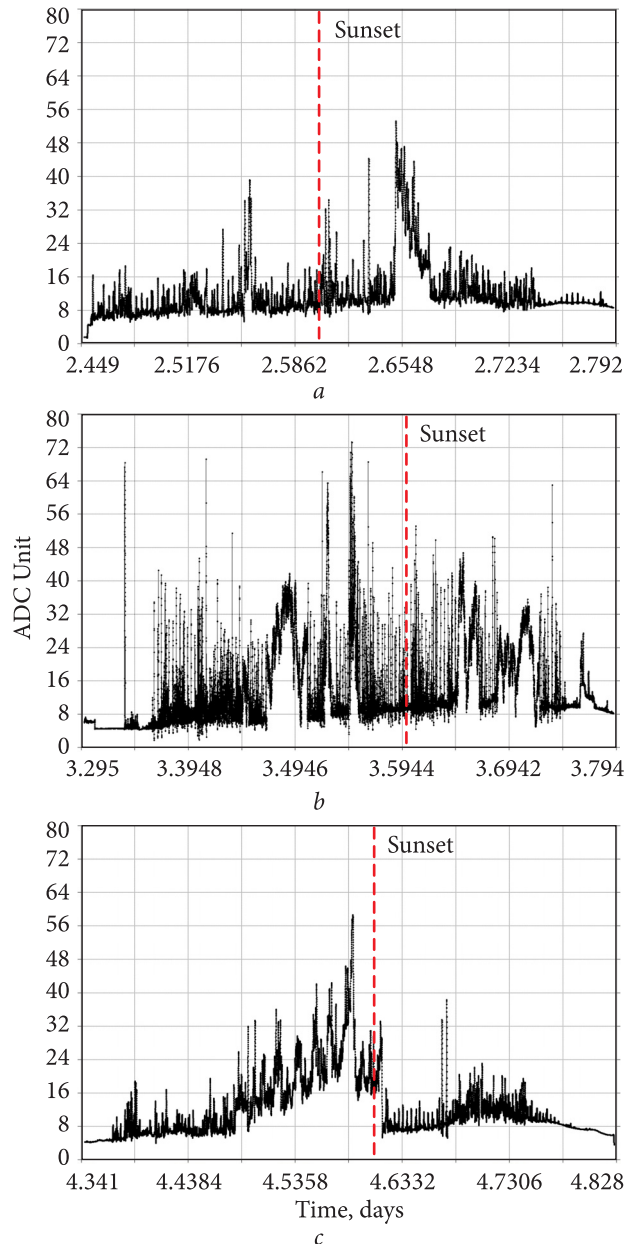


Fig. 2. The figure presents RFI recordings on the control day November 2, 2013 (a); on the day of the eclipse, November 3, 2013 (b); and on the following day, November 4, 2013 (c). The dashed lines indicate approximate time moments of sunset in Odesa

Under normal solar conditions, the ionospheric D-layer (altitude of 60–90 km) contributes to the radio wave absorption in the range of 10–30 MHz. During an eclipse, the flux of ultraviolet radiation nearly vanishes, and is significantly weakened within the penumbral zone, which leads to a rapid decline in electron density in the D-layer. As a result, absorption at 25 MHz may be slightly reduced (by fractions of a decibel) within the lunar shadow region. Addi-

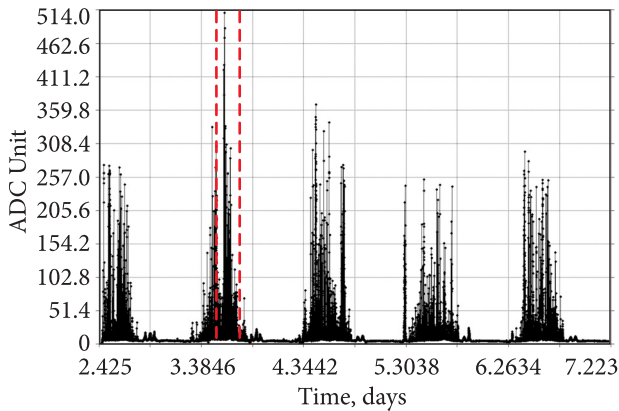


Fig. 3. Raw, unprocessed, and unsmoothed full-power signal data in terms of ADC counts at a frequency of 25 MHz (linear polarization A), recorded by the URAN-4 from November 2 to November 7, 2013. The dashed lines indicate an approximate occurrence interval for the solar eclipse on November 3, 2013

tionally, the passage of atmospheric acoustic-gravity waves propagating horizontally over hundreds of kilometers can induce localized fluctuations in electron density in the *E* and *F* layers far from the main shadow and penumbra. These fluctuations may alter the reflection conditions for ground-based signals, allowing the antenna to receive transmissions from distant radio stations and broadband interference sources that would normally fall outside the antenna's reception pattern.

However, without incorporating data from other phased antenna arrays within the URAN system, it is difficult to draw broader conclusions regarding the nature of the observed effect. Further comparative analyses are planned to address this limitation.

3.2. Scintillations of cosmic radio sources on the day of the solar eclipse

Scintillations of radio emission from the source 3C 123 (a radio galaxy) at 25 MHz were analyzed on the day of the solar eclipse (November 3, 2013), over a range of time periods from 10 seconds to 3.6 minutes, as well as signals from the Cas-A (a supernova remnant) within the 1–10 minutes range. The geomagnetic conditions during the days in 2013 subjected to the analysis were quiet, Kp3– on November 3 (day of the eclipse), Kp2+ on November 4, and Kp2– on November 5.

The recording session for the 3C 123 on the eclipse day began at 23:53 GMT and ended at 05:13 GMT,

thus having been ended 4 hours and 51 minutes prior to the onset of the eclipse. Observation graphs for the Cas-A are shown in Fig. 4, after smoothing with a cubic spline. For clarity, both graphs Fig. 4, *a* and *b* are plotted using the same Y-axis scale. The recording interval for Cas-A spanned from 19:12 to 23:02 GMT, beginning 3 hours and 44 minutes after the lunar shadow had passed. As evident from Fig. 4, the scintillations of Cas-A were relatively intense, suggesting that the ionosphere remained in an excited state for several hours following the end of the solar eclipse.

A comparison with Cas-A scans obtained on October 31, 2013 reveals that scintillations on that day were very weak, with the signal profile resembling a near-sinusoidal shape. However, it should be noted that similar scintillation patterns and intensities for Cas-A under quiet geomagnetic conditions were observed on multiple days both before and after the eclipse. Therefore, it is not possible to conclusively attribute the increased scintillation intensity of Cas-A on the eclipse day solely to the eclipse, based on URAN-4 data alone. The observed enhancement may simply be a coincidental occurrence.

The wavelet spectrum shown in Fig. 5, *a* indicates elevated "ionospheric activity" prior to the eclipse, with the radio source 3C 123 exhibiting intense scintillations across a broad range of periods, extending down to 20 seconds. On November 4, 2013 (Fig. 5, *c*), scintillations from 3C 123 persisted with only slightly reduced intensity compared to the pre-eclipse period, while the dominant "scintillation periods" increased to 35 seconds. On November 5, 2013, as illustrated in Fig. 5, *b*, ionospheric scintillations from 3C 123 were weaker than on the previous two days, with periods extending to 44 seconds. Figure 5, *d* presents the wavelet spectrum of Cas-A on November 4, 2013, the day following the eclipse (observation interval: 19:56–21:58 GMT), showing irregular scintillation behavior.

From the wavelet spectra of 3C 123, it is difficult to draw definitive conclusions regarding the detection of eclipse-induced ionospheric wave activity. The observed scintillations resemble typical patterns recorded at the URAN-4 site, with similar shapes and periods occurring both before and after the eclipse. The increased scintillation intensity on the day following the eclipse is not conclusive either, as even during extended periods of geomagnetic quiet, the

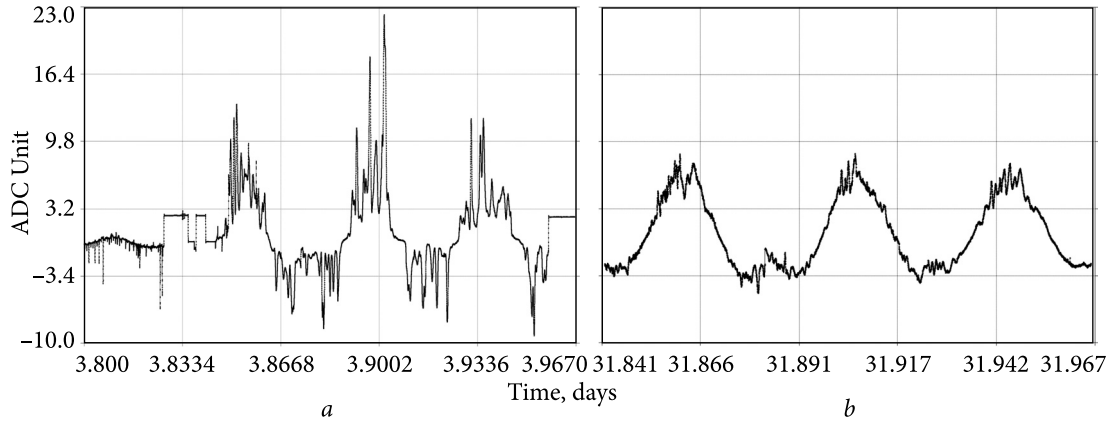


Fig. 4. Scans of the radio source Cas-A (Cassiopeia A) at a frequency of 25 MHz (modulation channel). Rectangular segments on the graph indicate calibration steps from the noise generator (a). Scans of Cas-A at 25 MHz (modulation channel) obtained on the control day of October 31, 2013 (b)

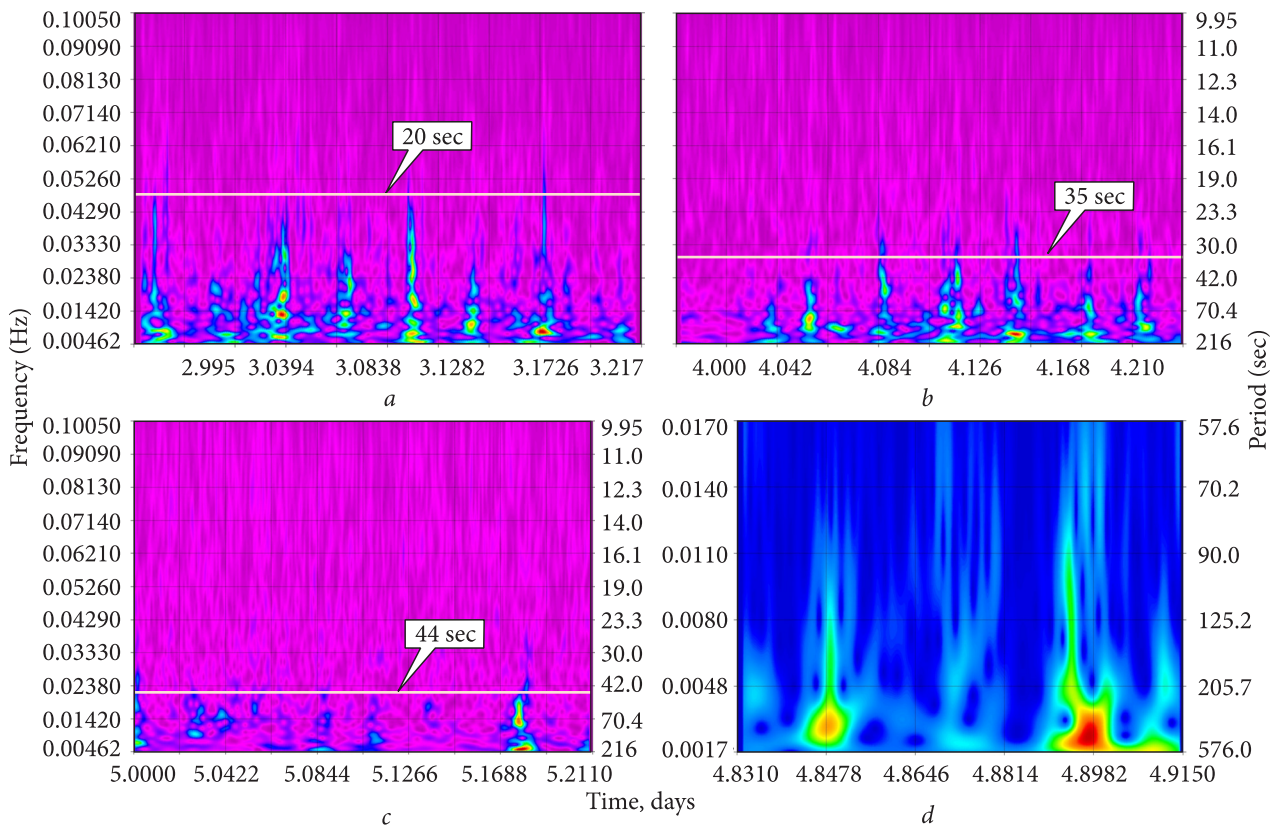


Fig. 5. Wavelet spectra from the radio source 3C 123 (within a band of time periods between 10 seconds and 3.6 minutes): a – November 3, 2013; b – the following day, November 4, 2013; c – November 5, 2013; d – is the wavelet spectrum of the radio source Cas-A, November 4, 2013

intensity and structure of scintillation wavelet spectra vary from day to day and lack consistent patterns.

Turning to the wavelet spectrum of Cas-A (several hours after the eclipse), we observe pronounced scintillations with quasi-periodic flux variations (Fig. 6). As can be seen, unlike the scintillations of

the 3C 123 that were observed prior to the day of the solar eclipse, the post-eclipse scintillations of Cas-A exhibit several quasi-harmonic components (highlighted by rectangles). Oscillations with a period of approximately 7 minutes persisted for 30 minutes, while those with a 3.4-minute period lasted 13 min-

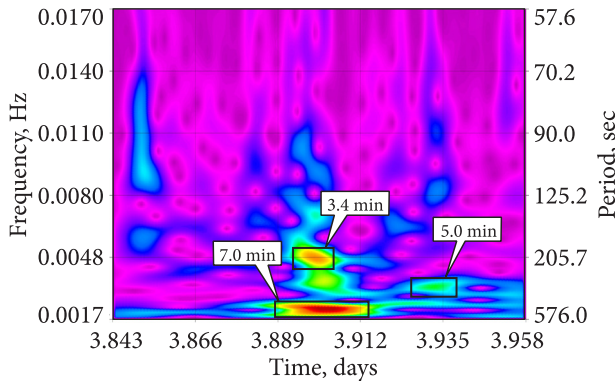


Fig. 6. Wavelet spectrum of scintillations from the radio source Cas-A at a frequency of 25 MHz after the solar eclipse

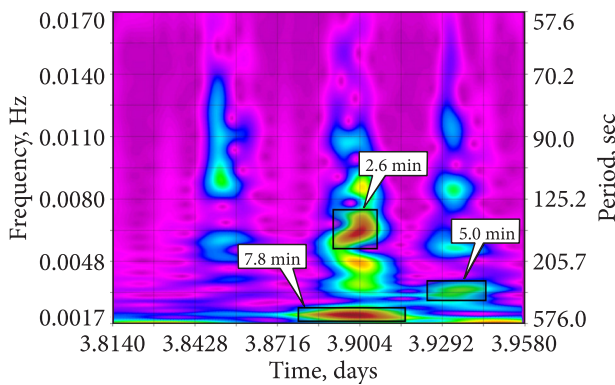


Fig. 7. Wavelet spectrum of scintillations from the radio source Cas-A at a frequency of 20 MHz. In the figure, rectangular markers highlight signal variability components with characteristic periods of approximately 7.8 minutes, 2.6 minutes, and 5 minutes

utes. The latter period, being close to half that of the primary oscillation, suggests it may represent a harmonic of the main wave. Weaker flux oscillations with a 5-minute period continued for 15 minutes.

It seems plausible that the observed effect was caused by Traveling Ionospheric Disturbances (TIDs) induced by acoustic-gravity waves still propagating through the URAN-4 antenna beam in the direction of Cas-A. The ionosphere may have remained in an elevated activity state following the eclipse. The fact that this effect was recorded 3 hours and 44 minutes after the eclipse could reflect a propagation delay, during which the wave disturbances traveled from the eclipse path to the URAN-4 observation site.

The closest point along the path of the total solar eclipse on November 3, 2013 to the URAN-4 radio telescope was located in Gabon (Central Africa). The great-circle distance from Gabon to the Odesa region is approximately 5500 km. Considering the ob-

served delay of 3 hours and 44 minutes, the estimated propagation speed of acoustic-gravity waves in the ionosphere is approximately 409 m/s. This value is plausible, as typical propagation velocities of medium-scale Traveling Ionospheric Disturbances (TIDs) induced by acoustic-gravity waves with periods of 3–7 minutes range between 200 and 600 m/s.

Accordingly, the marked enhancement in scintillation intensity of Cas-A following the solar eclipse is clearly distinguishable when compared with the data of the reference day November 4, 2013, during which scintillations were also present but looked irregular and lacked any quasi-periodic components.

However, a detailed assessment of this hypothesis, based on extensive observational data obtained with the URAN-4 phased antenna array, reveals that quasiperiodic variations in the wavelet spectra of the Cas-A have also been recorded on other geomagnetically quiet days, over different months of the year. This may hinder attribution of the wavelet spectral features observed, specifically to any eclipse-induced effects.

Therefore, while the hypothesis that the observed quasi-periodic scintillations could be generated by passage of acoustic-gravity waves appears physically reasonable — especially in the light of numerous studies on this topic — experience from the URAN-4 observations suggests that similar effects are not uncommon. Without corroborating data from other antennas within the URAN system, it is not possible to draw definite conclusions that the quasi-periodic scintillations observed in the Cas-A spectrum on November 3, 2013 were caused by TIDs originating along the track of the eclipse. The mildly excited state of the ionosphere several hours prior to the onset of the solar eclipse on November 3, 2013 — as inferred from scintillations of the source 3C 123 — may be attributed to the southward component of the interplanetary magnetic field B_z , measured at -5 nT.

Figure 7 presents, for comparison, the wavelet spectrum of scintillations from the radio source Cas-A at a frequency of 20 MHz, obtained on the day of the solar eclipse. Overall, the spectral structure resembles that observed at 25 MHz, though several minor differences are evident. The dominant quasi-period at 20 MHz is 7.8 minutes (with a duration of 41.7 minutes), while the expected harmonic peak has shifted to a "period" of 2.6 minutes (duration 20.0 minutes). The "period" of 5 minutes remains

unchanged (duration 25.0 minutes). Compared to the wavelet spectrum of Cas-A at 25 MHz, the oscillation durations corresponding to the identified "periods" at 20 MHz are slightly longer. In general, the similarity between the wavelet spectra at both frequencies supports the validity of the analysis.

4. Discussion

Similar effects were observed and investigated during the extensive campaign dedicated to the total solar eclipse of 2017, fully visible across the United States (The Great American Eclipse 2017), which involved thousands of amateur radio operators. Eclipse-related propagation anomalies were recorded within ± 0.3 hours at 1.8 MHz, ± 0.75 hours at 3.5 and 7 MHz, and ± 1 hour at 14 MHz. Numerous instances of enhanced radio communication over medium and long distances were confirmed, particularly at frequencies below 8 MHz. For 14 MHz, the observed signal propagation was consistent with refraction heights of $h < 125$ km [27].

It is noteworthy that observations of cosmic background radio intensity variations conducted with the URAN-4 array during the solar eclipse of June 10, 2021 (a partial phase was visible over Ukraine) at 20 and 25 MHz also revealed increased interference levels in recordings of galactic background emission — both during the eclipse and on the following day, June 11, 2021 [28].

A somewhat different result was obtained during the solar eclipse over the United States on April 8, 2024. Findings from an American amateur radio operator [29] suggest that the approach of the eclipse toward totality may facilitate long-distance reception of signals in the 10 and 14 MHz bands — both during and after the eclipse — compared to conditions observed prior to maximum solar obscuration.

Thus, each solar eclipse imprints a unique "signature" on the Earth's ionosphere and radio wave propagation. However, the use of a single antenna array, as in the case of URAN-4, does not allow for detailed characterization of the observed interference enhancement. To achieve this, simultaneous operation of multiple antenna arrays within the URAN system is required, along with cross-spectral analysis of scintillations time series.

The deployment of a radiometer designed and built by IRA NASU engineer V.V. Galanin, com-

pared with the successful implementation of a novel semi-automated observation analysis technique for detecting ionospheric scintillations of radio signals from cosmic sources using URAN-4, enabled the application of this antenna system to eclipse-related ionospheric studies. During the solar eclipse of November 3, 2013, the URAN-4 recorded increased interference levels on the day of the eclipse, with elevated interference persisting into the following day. This phenomenon is not easy to interpret, given that the eclipse was not visible from Ukrainian territory.

Therefore, we proceed to consider selected studies by other authors that explore the global impact of solar eclipses on the Earth's ionosphere and long-distance radio wave propagation.

In study [30], observations of the solar eclipse on April 8, 2024 revealed significant spatial variations in electron density, based on corresponding measurements. Data from the "Swarm" satellite indicated a 22% change in electron density as a function of latitude, reflecting the latitudinal influence of the eclipse on ionospheric conditions. In contrast, the "COSMIC-2" satellite reported a more pronounced 66% variation in electron density with altitude, highlighting the vertical structuring of the ionosphere during the eclipse. These findings clearly demonstrate the complex spatial impact of solar eclipses on the Earth's ionosphere.

Analysis of VLF signal amplitude profiles revealed substantial changes during the eclipse, indicating its influence on ionospheric propagation paths. For paths received in southeastern Virginia, USA, positive amplitude variations were observed for transmitters NPM, NML, and NLK, with a maximum recorded increase of 0.5986 dB for NPM. By comparison, a negative amplitude change of -5.25 dB was noted for NAA.

Unique effects were observed for VLF signals received in Fife, Scotland, where the receiver did not register a direct eclipse signature. Nevertheless, propagation paths from NAA and NSY responded to the eclipse, resulting in positive amplitude changes of 7.05 and 7.57 dB, respectively. These observations underscore the intricate relationship between radio wave propagation characteristics and eclipse-induced ionospheric modifications, which vary depending on geographic location and path-specific factors.

Reduced ionization in the D-region significantly alters the reflective properties of the waveguide for

paths intersecting the eclipse zone. Lower electron density and decreased collision frequency enhance reflection efficiency, allowing signals to propagate with reduced attenuation. This often leads to positive amplitude changes. Conversely, paths affected by phase distortions due to spatially non-uniform ionospheric variations may exhibit negative amplitude shifts.

Study [31] investigated magnetospheric currents, ionospheric conductivity, thermospheric winds, and electron precipitation during the "polar" solar eclipse of June 10, 2021. The results demonstrated that, through magnetosphere-ionosphere current coupling, the eclipse in the Northern Hemisphere induced electrodynamic changes in the Southern Hemisphere ionosphere, despite the absence of direct solar obscuration. This finding supports the hypothesis that a localized eclipse can trigger global electrodynamic effects across the Earth, whereby a local conductivity perturbation at one pole rapidly propagates changes in electric fields and currents to the opposite polar region, far beyond the eclipse shadow.

In study [32], a model of thermospheric wave activity (the upper atmospheric layer above the mesosphere, where temperature begins to rise sharply above 80–100 km, due to absorption of solar ultraviolet and X-ray radiation) revealed that fast bow waves are generated immediately following the onset of eclipse shadow motion. These waves closely track the shadow's trajectory. However, as the shadow advances and the bow waves interact with the background atmosphere, they gradually evolve into slower, large-scale Traveling Atmospheric Disturbances (TADs), which propagate more independently. This transformation explains why large-scale, slower wave structures are observed hundreds of kilometers away from the eclipse path.

The study shows that the eclipse shadow initiates wave processes that efficiently redistribute energy and momentum throughout the thermosphere, leading to changes in temperature and density at distances extending thousands of kilometers from the lunar shadow trajectory.

Study [33] examines the physics of wave disturbances generated by the solar eclipse of August 21, 2017, focusing on the simultaneous generation of long-wavelength and short-wavelength Traveling Ionospheric Disturbances (TIDs). To investigate these phenomena, researchers utilized data from a

dense network of "GNSS" receivers across the United States. Large-scale waves with wavelengths exceeding 400 km and periods of approximately 60–90 minutes were recorded; these are generated by the supersonic motion of the total lunar shadow and propagate outward in the form of diverging arcs. Concurrently, smaller-scale waves with wavelengths ranging from 50 to 200 km and shorter periods of 20–30 minutes were detected, originating over a much broader area corresponding to the lunar penumbra. These shorter waves are likely driven by gravitational instability or convective processes within the atmospheric column undergoing cooling over the extensive penumbral region. The study emphasizes that multi-antenna observations are essential for detecting and characterizing such subtle ionospheric effects.

In study [34], data from the "SuperDARN" high-frequency radar network were employed to investigate the dynamic ionospheric response to the total solar eclipse of April 8, 2024. A sharp disappearance of radar echoes was observed in regions covered by the eclipse shadow, confirming a collapse of ionization in the *E*-layer. The most significant result was the direct observation of pronounced disturbances in plasma drift velocities and vortex-like structures, indicating the generation of strong localized electric fields along the shadow boundaries. TIDs were also identified as characteristic oscillations in the radar data.

These lines of research suggest that the observed increase in radio-interference intensity during solar eclipses at considerable distances from the eclipse zone has a complex origin and remains insufficiently studied using large phased antenna arrays such as URAN-4. The effect is likely attributable to reduced ionospheric absorption and increased reflection height — extending the propagation path of ground-based signals — thus enabling reception at URAN-4 of signals that were previously significantly attenuated. Notably, the edge of the lunar penumbral path passed slightly south of the Crimean Peninsula, yet the effect was still detected.

The total solar eclipse of March 29, 2025 presented valuable opportunities for studying the spatial distribution of wave processes in the ionosphere in close proximity to the URAN and GURT systems of the Institute of Radio Astronomy of NASU. This facilitated an international eclipse observation campaign involving the LOFAR telescope of the International

Ventspils Radio Astronomy Center in Latvia and the KAIRA decameter radio telescope of the Sodankylä Observatory in Finland, both located within the partial eclipse zone. Additional important data was provided by geomagnetic field variation records from the magnetic observatories of the Institute of Geophysics of NASU and the magnetometer installed at the URAN-4 radio telescope.

Conclusions

This study presents results of an observational program conducted by V.V. Galanin at the URAN-4 radio telescope of the Institute of Radio Astronomy of NASU, aimed at investigating the effects of the hybrid total solar eclipse of November 3, 2013. Observations at 20 and 25 MHz, based on measurements of the low-frequency galactic radio background and interference intensities from October 31 to November 7, 2013, revealed an anomalous increase in radio-interference levels on the day of the eclipse, namely November 3, 2013. The interference peak was the highest among those recorded during the entire observational period, with elevated levels still persisting on November 4, 2013.

Scintillations of the radio source 3C 123 observable before and after the eclipse never exhibited any features that could be attributed to eclipse-related effects. Although quasi-periodic scintillations of the source Cas-A were notably intense compared with the levels of the reference day of October 31, 2013, such activity is not uncommon even under magnetically quiet conditions, according to the URAN-4 observation archive. Therefore, the observed spike in Cas-A scintillation on the day of the eclipse is most likely a coincidental occurrence.

Acknowledgments. The present research has been supported by the state Contract No. 4.1/25-P targeted at implementing the project "Global monitoring of radio signals of natural and artificial origin at decameter and meter wavelengths in the interests for cosmology and applied problems of defense capability".

A. Sukharev has been supported by the Postdoctoral research grant No. 1.1.1.9/LZP/1/24/048 "Research on Space Weather During Solar Cycle 25 as Observed Along the "Struve Geodetic Arc", that is implemented at the Ventspils University of Applied Sciences and is co-financed by the European Regional Development Fund.

REFERENCES

1. Galanin, V.V., Komendant, V.H., Yasinski, V.V., 2021. Observation control device for the Uran-4 decameter radio telescope. *Odessa Astronomical Publications*, **34**, pp. 74–75. DOI: 10.18524/1810-4215.2021.34.244382
2. Chernogor, L.F., 2013. *Physical effects of solar eclipses in atmosphere and geospace*. Monograph. Kharkiv: V.N. Karazin Kharkiv National University Publ. 480 p.
3. Lion, E.F., Bridge, H.S., Binsack, J.H., 1967. Explorer-35 Plasma Measurements in Vicinity of the Moon. *J. Geophys. Res.*, **72**(23), pp. 6113–6117. DOI: 10.1029/JZ072i023p06113
4. Ness, N.F., 1970. *Interaction of the Solar Wind with the Moon*. Preprint NASA-GSFC, X-692 70-141, Maryland
5. Interaction of the Solar Wind with the Terrestrial Planets. Section: The Solar Wind in the Near-Earth Environment. Studies of the Solar Wind Flow around the Moon. 1988. *Adv. Sci. Technol. Ser. Astronomy*, **35**.
6. Chernogor, L.F., Barabash, V.V., 2011. The response of the middle ionosphere to the solar eclipse of 4 January 2011 in Kharkiv: some results of vertical sounding. *Kosm. nauka tehnol.*, **17**(4), pp. 41–52. DOI: 10.15407/knit2011.04.041
7. Typinski, D., Greenman, W., 2015. Things That Go Hump in the Night – A Fun Experiment [pdf]. *NASA RadioJove Project*. Available from: https://radiojove.gsfc.nasa.gov/radio_telescope/observing/observing_galactic_bkg.pdf
8. Mertsch, P., Sarkar, S., 2013. Loops and spurs: the angular power spectrum of the Galactic synchrotron background. *J. Cosmol. Astropart. Phys.*, **06**, 041. DOI: 10.1088/1475-7516/2013/06/041
9. Rapoport, Yu.G., Cheremnykh, O.K., Koshovyy, V.V., Melnik, M.O., Ivantyshyn, O.L., Nogach, R.T., Selivanov, Yu.A., Grimal'sky, V.V., Mezentsev, V.P., Karataeva, L.M., Ivchenko, V.M., Milinevsky, G.P., Fedun, V.N., Tkachenko, Ye.N., 2017. Ground-based acoustic parametric generator impact on the atmosphere and ionosphere in an active experiment. *Ann. Geophys.*, **35**(1), pp. 53–70. DOI: 10.5194/angeo-35-53-2017
10. Galanin, V.V., Inyutin, G.A., Kvasha, I.M., Panishko, S.K., Pisarenko, Ya.V., Rashkovskij, S.L., Ryabov, M.I., Serokurova, N.G., Tsevevich, V.P., Sharykin, N.K., 1989. URAN-4 radio telescope as an element of VLBI system. *Kinematika i Fizika Nebesnykh Tel*, **5**, pp. 87–90.
11. Lytvynenko, O.A., Panishko, S.K., Derevyagin, V.G., 2023. The Long-Term Observations of the Power Cosmic Radio Sources on the Radio Telescope URAN-4 at the Decameter Wave Range. *Odessa Astronomical Publications*, **36**, pp. 118–121. DOI: 10.18524/1810-4215.2023.36.290139

12. Sukharev, A., Orlyuk, M., Ryabov, M., Sobitniak, L., Bezrukovs, V., Panishko, S., Romenets, A., 2022. Results of comparison of fast variations of geomagnetic field and ionospheric scintillations of 3C 144 radio source in the area of Odessa geomagnetic anomaly. *Astron. Astrophys. Trans.*, **33**(1), pp. 67–88. DOI: 10.17184/eac.6481
13. Madden, H.H., 1978. Comments on the Savitzky-Golay convolution method for least-squares-fit smoothing and differentiation of digital data. *Anal. Chem.*, **50**(9), pp. 1383–1386. DOI: 10.1021/ac50031a048
14. Breaz, N., 2004. The cross-validation method in the smoothing spline regression. *Acta Universitatis Apulensis* 7. ResearchGate. Available from: https://www.researchgate.net/publication/237262065_THE_CROSS-VALIDATION_METHOD_IN_THE_SMOOTHING_SPLINE_REGRESSION
15. Garimella, R.V., 2017. A Simple Introduction to Moving Least Squares and Local Regression Estimation. Report number: LA-UR-17-24975. United States, DOI: 10.2172/1367799
16. Tipton, C., 2022. Basics of Fourier Analysis of Time Series Data. *Johnson Matthey Technol. Rev.*, **66**(2), pp. 169–176. DOI: 10.1595/205651322X16433652085975
17. Popinski, W., Kosek, W., 1995. The Fourier transform band pass filter and its application for polar motion analysis. *Artif. Satell., Planet. Geod.*, **24** (30(1)), pp. 9–25.
18. Allen, J., 1977. Short term spectral analysis, synthesis, and modification by discrete Fourier transform. *IEEE Trans. Acoust. Speech Signal Process.*, **25**(3), pp. 235–238. DOI: 10.1109/TASSP.1977.1162950
19. Wang, Yun, He, Ping, 2023. Comparisons between fast algorithms for the continuous wavelet transform and applications in cosmology: the 1D case. *RAS Tech. Instrum.*, **2**(1), pp. 307–323. DOI: 10.1093/rasti/rzad020
20. Scholl, S., 2021. *Fourier, Gabor, Morlet or Wigner: Comparison of Time-Frequency Transforms*. DOI: 10.48550/arXiv.2101.06707
21. NOAA Weekly Highlights and 27-Day Forecast. Available from: <https://www.swpc.noaa.gov/products/weekly-highlights-and-27-day-forecast>; Users Guide to The Preliminary Report and Forecast of Solar Geophysical Data. Available from: https://www.swpc.noaa.gov/sites/default/files/images/u2/Usr_guide.pdf
22. Esaenwi, S., Ofodum, C.N., Okere, B.I., Opara, F.E., Sigalo, F.B., Omaliko, K.C., Wali, C.B., Sigalo, M.B., Suraju, S., Eze, E.J., Okonkwo, H., Osuji, U., Omowa, E., Ogbonda, C., and Anuforom, A., 2016. The 3 November 2013 partial solar eclipse: the effect of Nigeria media popularization. *Nig. J. Space Res.*, **14**(1), 5 p.
23. Patel, D.B., Kotadia, K.M., Lele, P.D., Jani, K.G., 1986. Absorption of radio waves during a solar eclipse. *Proc. Indian Acad. Sci. (Earth Planet. Sci.)*, **95**(2), pp. 193–200. DOI: 10.1007/bf02871864
24. Bamford, R.A., 2001. The effect of the 1999 total solar eclipse on the ionosphere. *Phys. Chem. Earth (C)*, **26**(5), pp. 373–377. DOI: 10.1016/S1464-1917(01)00016-2
25. Knižova, K.P., Mošna, Z., 2011. Acoustic-Gravity Waves in the Ionosphere during Solar Eclipse Events. In: Beghi, M.G. ed., 2011. *Acoustic Waves – From Microdevices to Helioseismology*. ISBN: 978-953-307-572-3, InTech. Available from: <http://www.intechopen.com/books/acoustic-waves-from-microdevices-to-helioseismology/acoustic-gravity-waves-in-the-ionosphere-during-solar-eclipse-events>
26. Kaladze, T.D., Pokhotelov, O.A., Shah, H.A., Khan, M.I., Stenflo, L., 2008. Acoustic-gravity waves in the Earth's ionosphere. *J. Atmos. Sol.-Terr. Phys.*, **70**(13), pp. 1607–1616. DOI: 10.1016/j.jastp.2008.06.009
27. Nayak, Ch., Yiğit, E., 2018. GPS-TEC Observation of Gravity Waves Generated in the Ionosphere during 21 August 2017 Total Solar Eclipse. *J. Geophys. Res. Space Phys.*, **123**(1), pp. 725–738. DOI: 10.1002/2017JA024845
28. Sukharev, A.L., Ryabov, M.I., Galanin, V.V., Komendant, V.G., 2023. About research programs at the radio telescope "URAN-4" IRA NASU – monitoring of fluxes of powerful radio sources, study of the Sun's supercorona, observations of solar eclipse. *Odessa Astronomical Publications*, **36**, pp. 135. DOI: 10.18524/1810-4215.2023.36.290143
29. Chernogor, L.F., 2016. Propagating waves and processes associated with the March 20, 2015 solar eclipse in the ionosphere over Europe. *Kinemat. Phys. Celest. Bodies*, **32**(4), pp. 60–72.
30. Kaladze, T.D., Pokhotelov, O.A., Shah, H.A., Khan, M.I., Stenflo, L., 2008. Acoustic-gravity waves in the Earth's ionosphere. *J. Atmos. Terr. Phys.*, **70**(13), pp. 1607–1616. DOI: 10.1016/j.jastp.2008.06.009
31. Crowley, G., Azeem, S.M.I., 2018. Extreme Ionospheric Storms and Their Effects on GPS Systems. In book: Buzulukova, N. ed., 2018. *Extreme Events in Geospace*. Elsevier, 2018, pp. 555–586. DOI: 10.1016/B978-0-12-812700-1.00023-6
32. Kozyreva, O., Kozlovsky, A., Pilipenko, V., Yagova, N., 2019. Ionospheric and geomagnetic Pc5 oscillations as observed by the ionosonde and magnetometer at Sodankylä. *Adv. Space Res.*, **63**(7), pp. 2052–2065. DOI: 10.1016/j.asr.2018.12.004
33. Eisenbeis, J., 2020. *Ionospheric Dynamics by GNSS total electron content observations: the effect of Solar Eclipses and the mystery of Earthquake precursors*. Doctoral thesis in Earth and Environmental Sciences. Université Paris Cité, 2020. English. NNT: 2020UNIP7027. Available from: https://theses.hal.science/tel-03181359v1/file/EISENBEIS_Julian_va2.pdf
34. Sun, Y.-Y., Shen, M.M., Tsai, Y.-L., Lin, C.-Y., Chou, M.-Y., Yu, T., Lin, K., Huang, Q., Wang, J., Qiu, L., Chen, C.-H., and Liu, J.-Y., 2021. Wave Steepening in Ionospheric Total Electron Density due to the 21 August 2017 Total Solar Eclipse. *J. Geophys. Res. Space Phys.*, **126**(3), e2020JA028931. DOI: 10.1029/2020JA028931

Received 25.02.2025

А.Л. Сухарев, М.І. Рябов, В.В. Галанін, Д.А. Забора
Одеська радіообсерваторія Інституту радіоастрономії НАН України
вул. Маразліївська, 1В, м. Одеса, 65014, Україна

ВПЛИВ СОНЯЧНОГО ЗАТЕМНЕННЯ
3 ЛИСТОПАДА 2013 РОКУ НА СТАН ІОНОСФЕРИ, ДОСЛІДЖЕНИЙ
ЗА ДОПОМОГОЮ РАДІОАСТРОНОМІЧНОГО МЕТОДУ

Предмет і мета роботи. У роботі розглянуто наслідки сонячного затемнення 3 листопада 2013 року, зокрема нетипове підвищення рівня радіочастотних завад та мерехтіння радіоджерел ЗС 123 та Cas-A на частоті 25 МГц. Ці явища могли бути спричинені підвищеною хвильовою активністю іоносфери під час затемнення та зниженням рівня іоносферного поглинання радіохвиль.

Методи та методологія. Спостереження випромінювання від космічних радіоджерел проводилися за допомогою низькочастотного радіотелескопа УРАН-4 (діапазон 10...30 МГц). Результати спостережень випромінювання від космічних радіоджерел та наявних у згаданому діапазоні завадових сигналів були подані у вигляді часових рядів для подальшої обробки і дослідження. Для визначення основних періодів мерехтіння радіоджерела до масивів даних було застосовано методи вейвлет-аналізу.

Результати. Значне збільшення інтенсивності завад було зареєстровано у день кульмінації затемнення, а також наступного дня. У радіоджерела Cas-A спостерігалися варіації інтенсивності, близькі до квазіперіодичних, з характерною тривалістю від 3 до 7 хвилин. Аналіз мерехтіння радіоджерела ЗС 123, проведений до і після затемнення, не надав достатніх даних для переконливих висновків про його вплив.

Висновки. Незважаючи на те, що сонячне затемнення 3 листопада 2013 року не було оптично видимим в Україні (оскільки найближча зона видимості часткового затемнення була розташована південніше Криму та у Туреччині), все ж зареєстроване аномальне підвищення рівня завад протягом часового вікна спостережень з 31 жовтня до 7 листопада 2013 року. Подібних посилень не спостерігалось ні до, ні після затемнення. Ймовірно, це явище було результатом комбінованого ефекту, який включав зменшення поглинання в *D*-шарі іоносфери, зміщення розташування *F*-шару (що спричинює далекі віддзеркалення) та появу активних агентів, таких як *TID*-хвилі. Усе це разом призвело до різкого збільшення рівня завад на частоті 25 МГц. Хоча затемнення не спостерігалось оптично, згенеровані ним іоносферні збурення досягли УРАН-4 і проявилися як потужний сплеск рівня завад при прийманні із зенітного напрямку.

Ключові слова: радіомерехтіння, іоносфера, іоносферна буря, геомагнітна буря, прояви сонячного затемнення в іоносфері, декаметрова радіоастрономія.